Supplement of Geosci. Model Dev., 16, 1277–1296, 2023
https://doi.org/10.5194/gmd-16-1277-2023-supplement

Geoscientific Model Development
Open Access
EGU

Supplement of

A new precipitation emulator (PREMU v1.0) for lower-complexity models

Gang Liu et al.

Correspondence to: Shushi Peng (speng@pku.edu.cn)

Table S1: Table for comparison of characteristics of GLAP and gridded precipitation between observations and emulations from Simple Linear and PREMU during the calibration (1901-1950) and validation period (1951-2016).

.

	Precipitation characteristics	GSWP3	Simple Linear	PREMU	Unit
Calibration	Average GLAP	1002	1002	1002	mm/yr
	Trend of GLAP	0.54	0.30	0.48	mm/yr^2
	Standard variation of GLAP	20.43	5.58	11.52	mm/yr
	Pearson correlation coefficient	\	0.27	0.81	\
	Proportion of grid cells with more than 25% error of MAP[a]	\	0.27%	0.29%	\
Validation	Average GLAP	1021	1023	1021	mm/yr
	Trend of GLAP	0.22	0.69	0.22	mm/yr^2
	Standard variation of GLAP	21.55	15.21	9.46	mm/yr
	Pearson correlation coefficient	\	0.15	0.67	\
	Proportion of grid cells with more than 25% error of MAP[b]	\	26.72%	16.83%	\

[a]: during 1901-1930**;** [b]: during 1987-2016

Table S2: Table for comparison of characteristics of GLAP and gridded precipitation between ESMs average and emulations from PREMU under the scenario of calibration (SSP5-8.5) and scenario of validation (SSP1-2.6; SSP2-4.5; SSP3-7.0).

	Precipitation characteristics	GSWP3	PREMU	Unit
Calibration: SSP5-8.5	Average GLAP	1066	1066	mm/yr
	Trend of GLAP	0.96	0.96	mm/yr^2
	Standard variation of GLAP	25.20	24.69	mm/yr
	Pearson correlation coefficient	\	0.98	\
	Proportion of grid cells with more than 10% error of MAP*	\	0.07%	\
Validation: SSP1-2.6	Average GLAP	1053	1043	mm/yr
	Trend of GLAP	0.29	0.16	mm/yr^2
	Standard variation of GLAP	11.38	6.50	mm/yr
	Pearson correlation coefficient	\	0.86	\
	Proportion of grid cells with more than 10% error of MAP*	\	8.41%	\
Validation: SSP2-4.5	Average GLAP	1055	1052	mm/yr
	Trend of GLAP	0.58	0.45	mm/yr^2
	Standard variation of GLAP	15.20	12.05	mm/yr
	Pearson correlation coefficient	\	0.95	\
	Proportion of grid cells with more than 10% error of MAP*	\	5.33%	\
Validation: SSP3-7.0	Average GLAP	1054	1059	mm/yr
	Trend of GLAP	0.69	0.76	mm/yr^2
	Standard variation of GLAP	19.10	19.55	mm/yr
	Pearson correlation coefficient	\	0.95	\
	Proportion of grid cells with more than 10% error of MAP[a]	\	5.48%	\

[a]: during 2071-2100.

Table S3: Percentage error of trend in GLAP from ESMs average and each ESM and its corresponding emulation by PREMU during the period 2015-2100 under four scenarios. The ESMs Average represents the multi-model mean precipitation predicted by gridded temperature from 9 ESMs. Note that the unit is mm $year^{-2}$.

Relative errors of trend in GLAP	SSP1-2.6	SSP2-4.5	SSP3-7.0	SSP5-8.5
ESMs average	-45%	-22%	10%	0%
UKESM1-0-LL	-48%	-21%	-1%	0%
MPI-ESM1-2-LR	-70%	17%	8%	0%
MIROC6	2%	-25%	19%	-1%
IPSL-CM6A-LR	-44%	-23%	-14%	0%
GFDL-ESM4	-139%	-85%	-125%	-28%
EC-Earth3	36%	14%	6%	1%
CanESM5	-21%	-21%	-1%	0%
CESM2	-63%	-33%	95%	-2%
ACCESS-ESM1-5	-53%	-12%	-10%	-4%

Figure S1. The corresponding results from the PCA of the gridded temperature in July between 1901 and 1950 from GSWP3: **a**) The cumulative variance explanation rate of the top ten principal components. **b-k**) Coefficients of the top ten principal components.

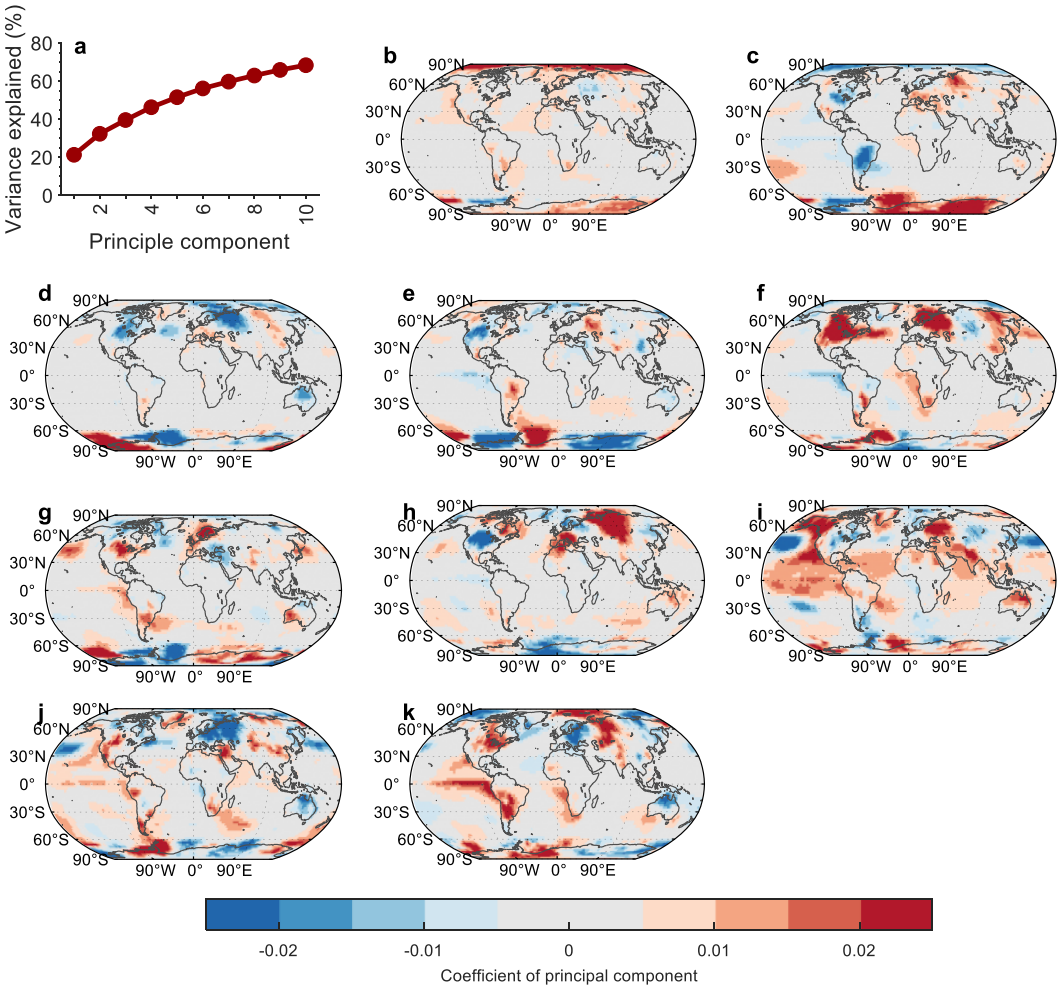

Figure S2. The corresponding results from the PCA of the gridded temperature in January between 2015 and 2100 from ESMs under SSP5-8.5 scenario: **a**) The average cumulative variance explanation rate of the top ten principal components in 9 ESMs. **b-k**) The average of coefficients of the top ten principal components across the nine ESMs.

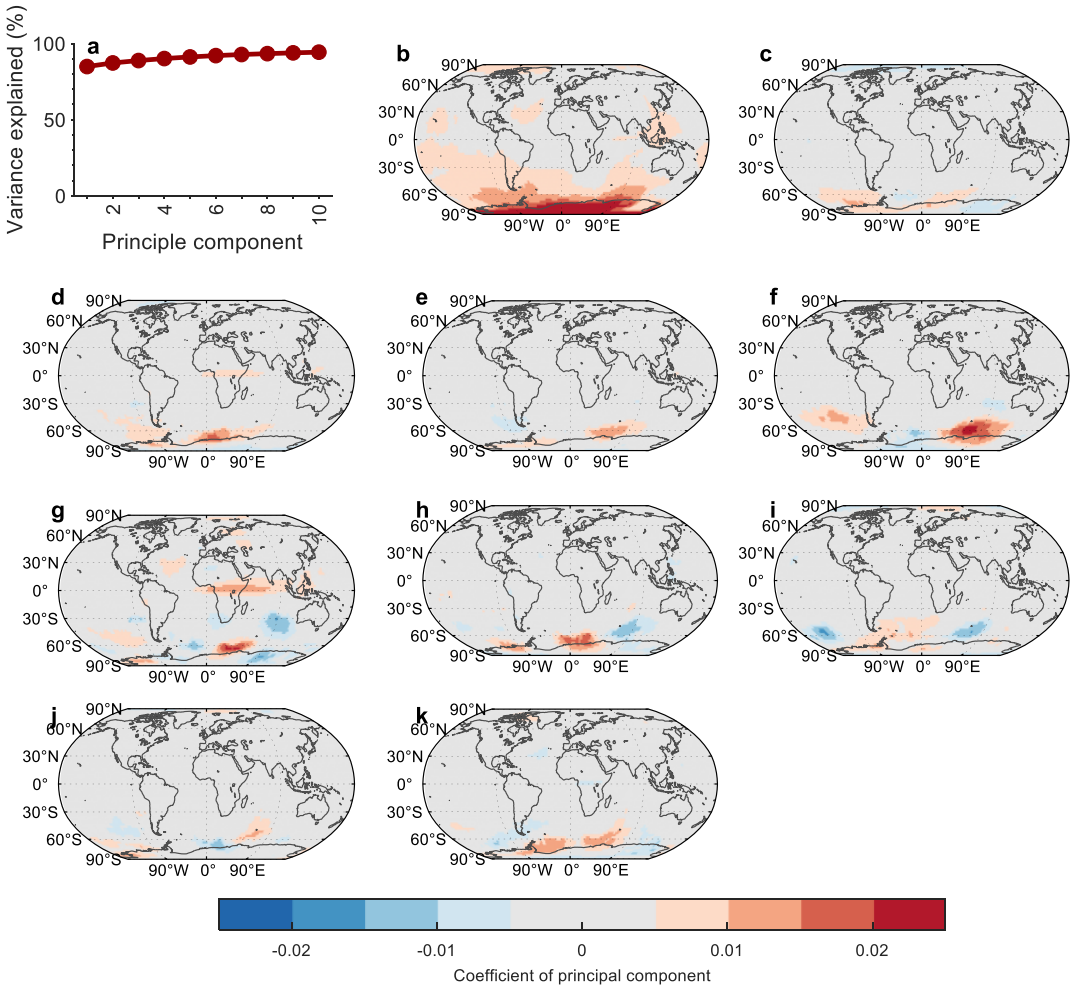

Figure S3. The corresponding results from the PCA of the gridded temperature in July between 2015 and 2100 from ESMs under SSP5-8.5 scenario: **a**) The average cumulative variance explanation rate of the top ten principal components in 9 ESMs. **b-k**) The average of coefficients of the top ten principal components in across the nine ESMs.

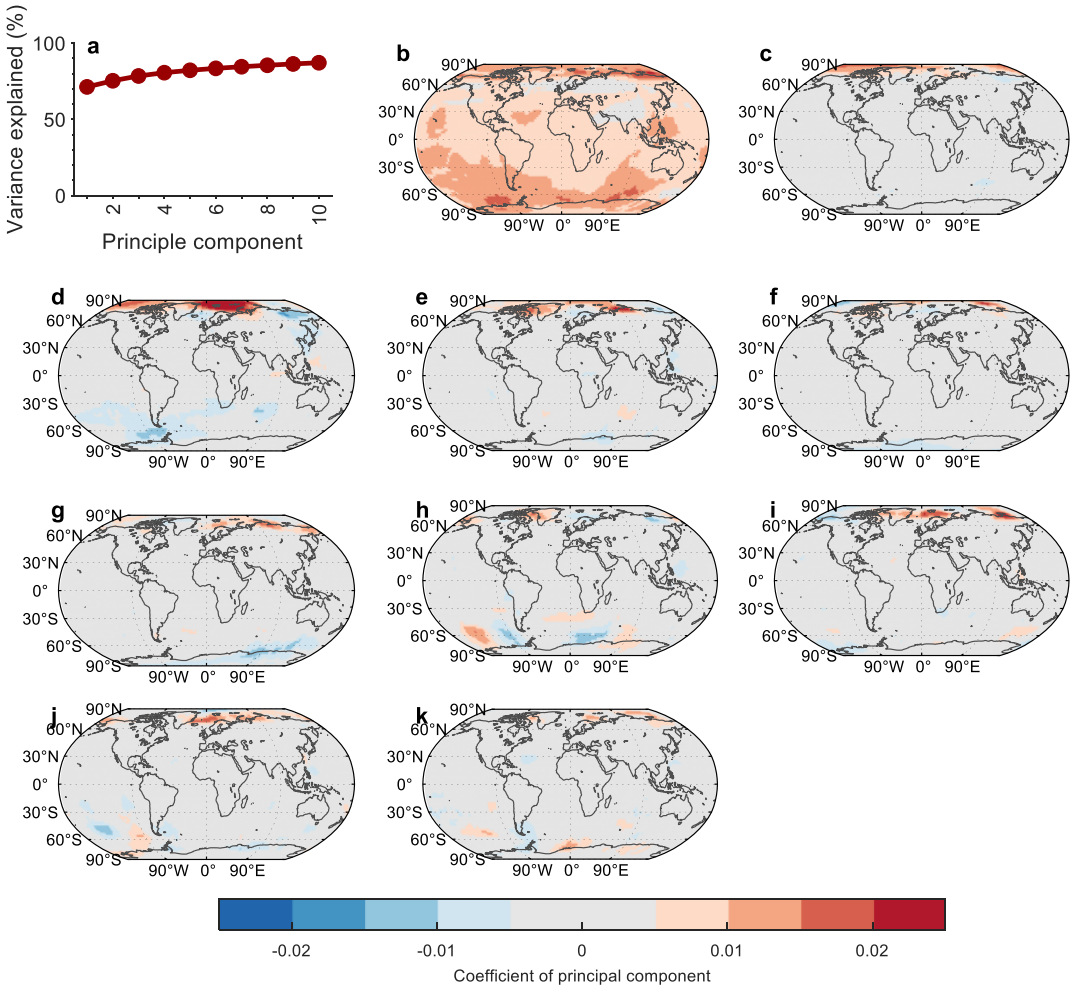

Figure S4. A heat map of the correlation coefficients between the annual mean of 10 PCs and 15 location-based climate indices from 1950 to 2016. The 15 climate indices are the Pacific North America Index (PNA); East Pacific/North Pacific Oscillation (EPNP); Western Pacific Index (WP); Eastern Asia/Western Russia (EAWR); North Atlantic Oscillation (NAO); two ENSO indices (Eastern Tropical Pacific SST, NINO 3; East Central Tropical Pacific SST, NINO 3.4); Tropical Northern Atlantic Index (TNA); Tropical Southern Atlantic Index (TSA); Western Hemisphere warm pool (WHWP); Oceanic Nino Index (ONI); Pacific Decadal Oscillation (PDO); North Pacific pattern (NP); Trans-Nino Index (TNI); Global Mean Land/Ocean Temperature Index (Mean T index). Data is available at https://psl.noaa.gov/data/climateindices/list/.

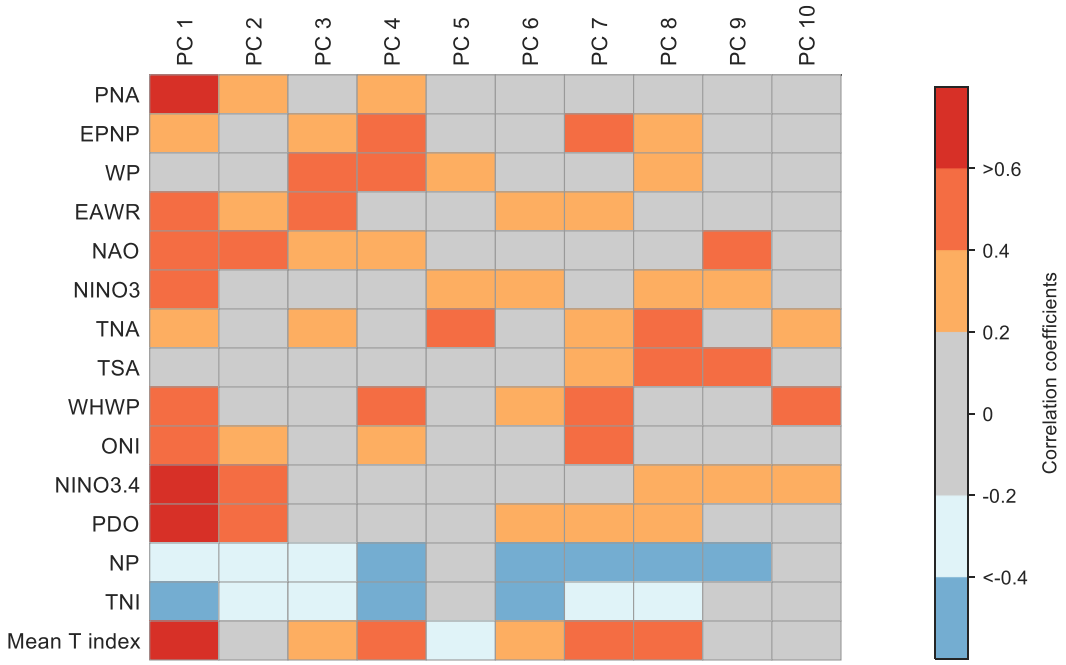

Figure S5. a) The differences in MAP between GSWP3 and emulations from PREMU. **b**) The differences in MAP between emulations from PREMU and Simple Linear method

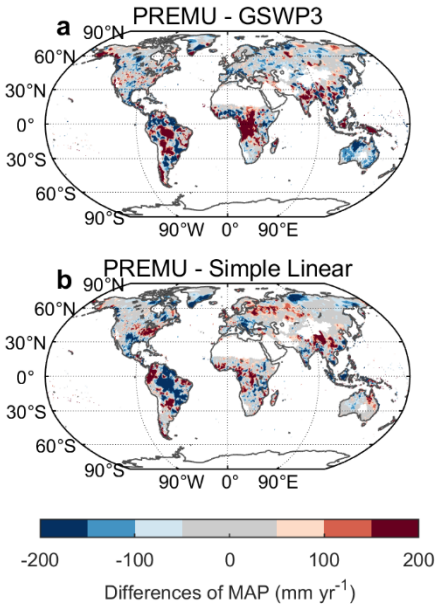

Figure S6. a) The differences in changes of MAP between GSWP3 and emulations from PREMU. **b**) The differences in changes of MAP between emulations from PREMU and Simple Linear method.

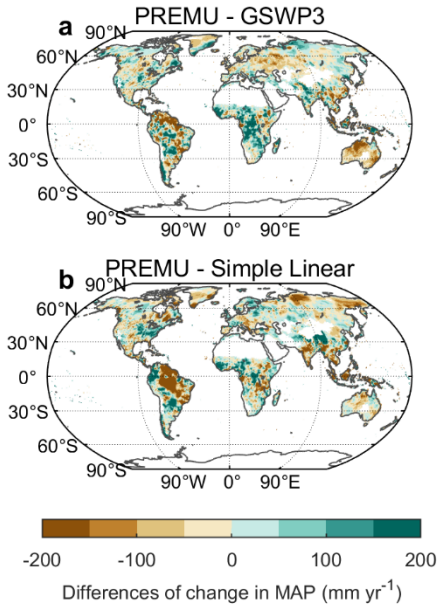

Figure S7. The anomaly of GLAP from each ESM under the SSP2-4.5 scenario: **a**) UKESM1-0-LL; **b**) MPI-ESM1-2-LR; **c**) MIROC6; **d**) IPSL-CM6A-LR; **e**) GFDL-ESM4; **f**) EC-Earth3; **g**) CanESM5; **h**) CESM2; **i**) ACCESS-ESM1-5.

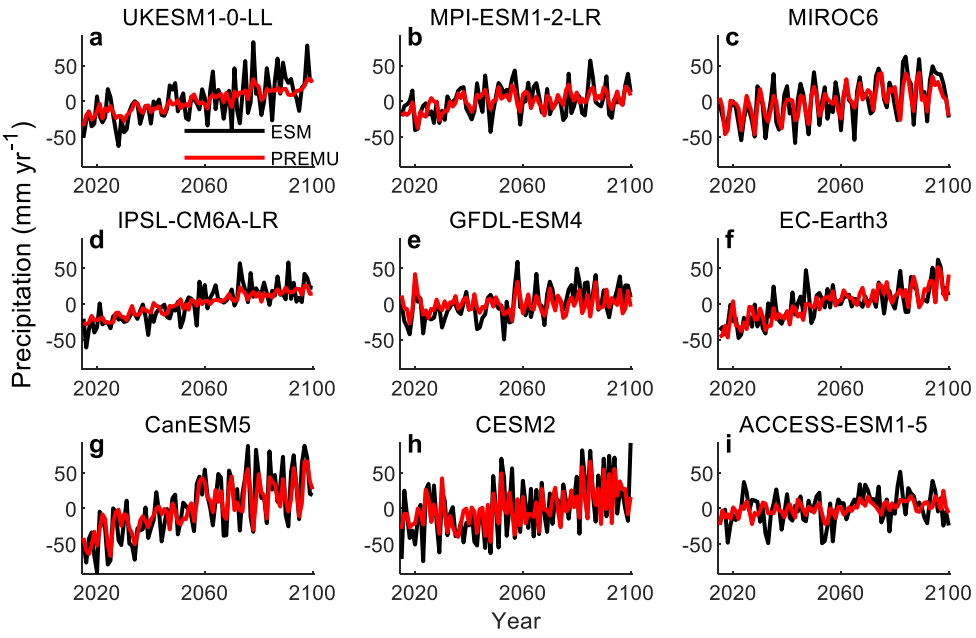

Figure S8. The anomaly of GLAP from each ESM under the SSP3-7.0 scenario: **a**) UKESM1-0-LL; **b**) MPI-ESM1-2-LR; **c**) MIROC6; **d**) IPSL-CM6A-LR; **e**) GFDL-ESM4; **f**) EC-Earth3; **g**) CanESM5; **h**) CESM2; **i**) ACCESS-ESM1-5.

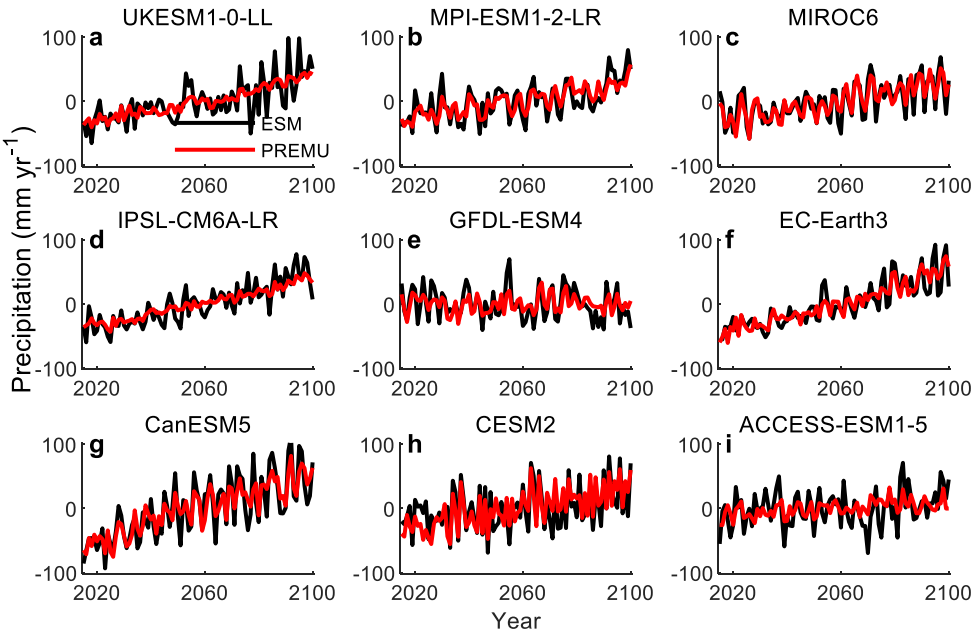

Figure S9. The anomaly of GLAP from each ESM under the SSP5-8.5 scenario: **a**) UKESM1-0-LL; **b**) MPI-ESM1-2-LR; **c**) MIROC6; **d**) IPSL-CM6A-LR; **e**) GFDL-ESM4; **f**) EC-Earth3; **g**) CanESM5; **h**) CESM2; **i**) ACCESS-ESM1-5.

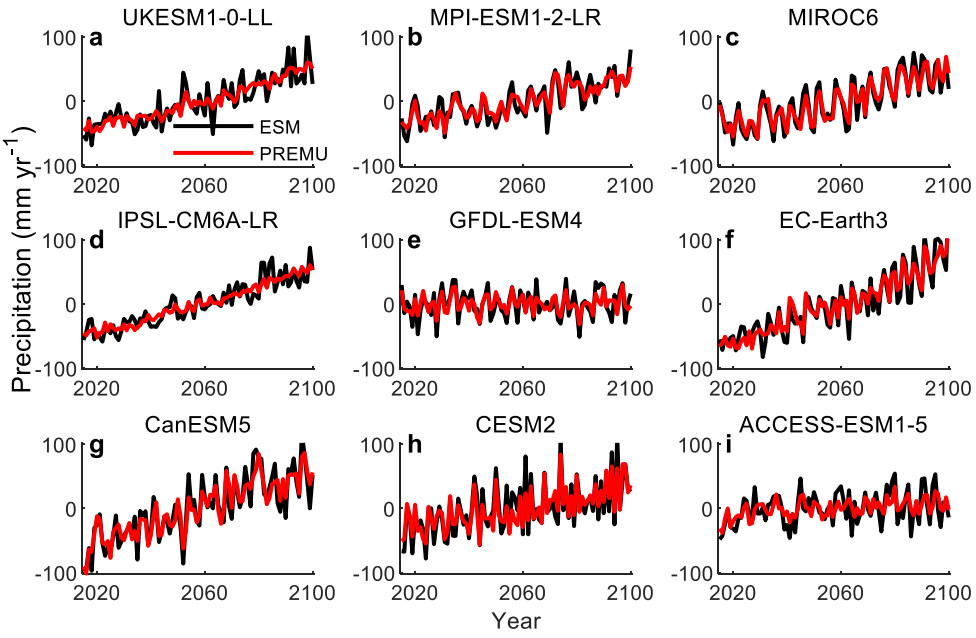

Figure S10. The spatial pattern of error of the MAP in 2071-2100 between each ESM and our emulation under the SSP2-4.5 scenario: **a**) UKESM1-0-LL; **b**) MPI-ESM1-2-LR; **c**) MIROC6; **d**) IPSL-CM6A-LR; **e**) GFDL-ESM4; **f**) EC-Earth3; **g**) CanESM5; **h**) CESM2; **i**) ACCESS-ESM1-5.

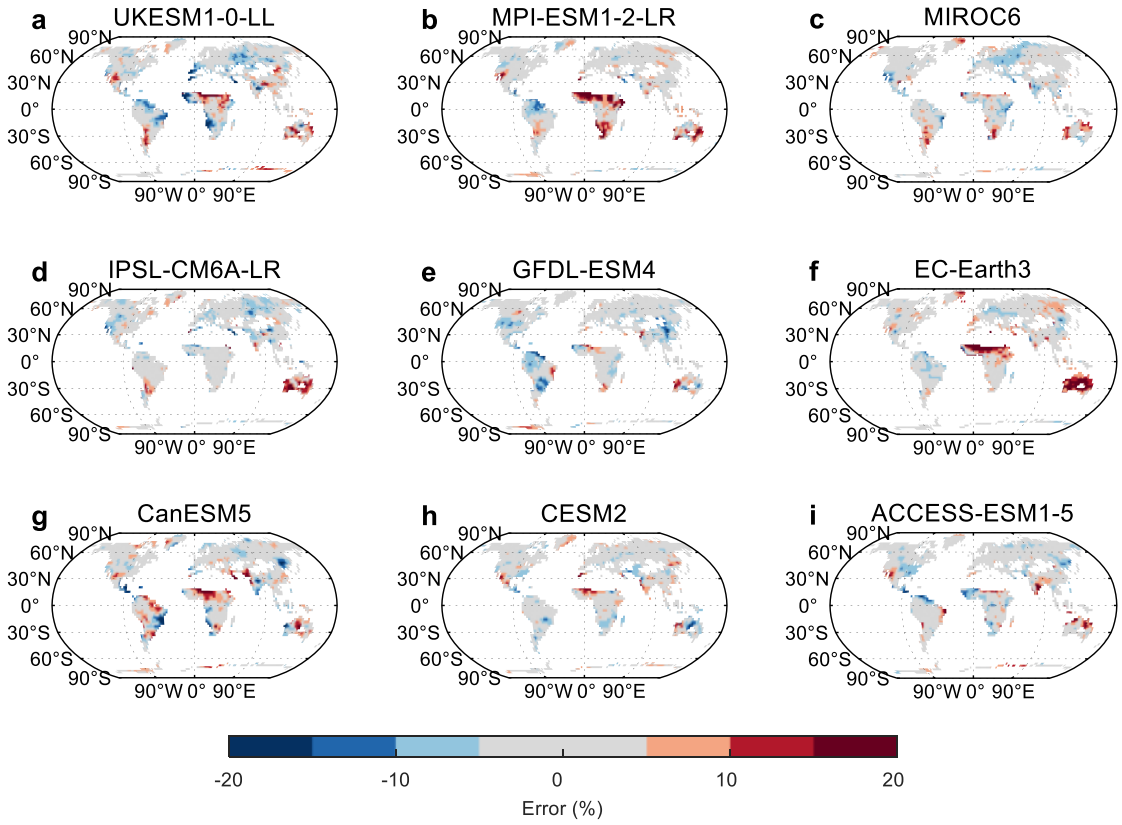

Figure S11. The spatial pattern of error of the MAP in 2071-2100 between each ESM and our emulation under the SSP3-7.0 scenario: **a**) UKESM1-0-LL; **b**) MPI-ESM1-2-LR; **c**) MIROC6; **d**) IPSL-CM6A-LR; **e**) GFDL-ESM4; **f**) EC-Earth3; **g**) CanESM5; **h**) CESM2; **i**) ACCESS-ESM1-5.

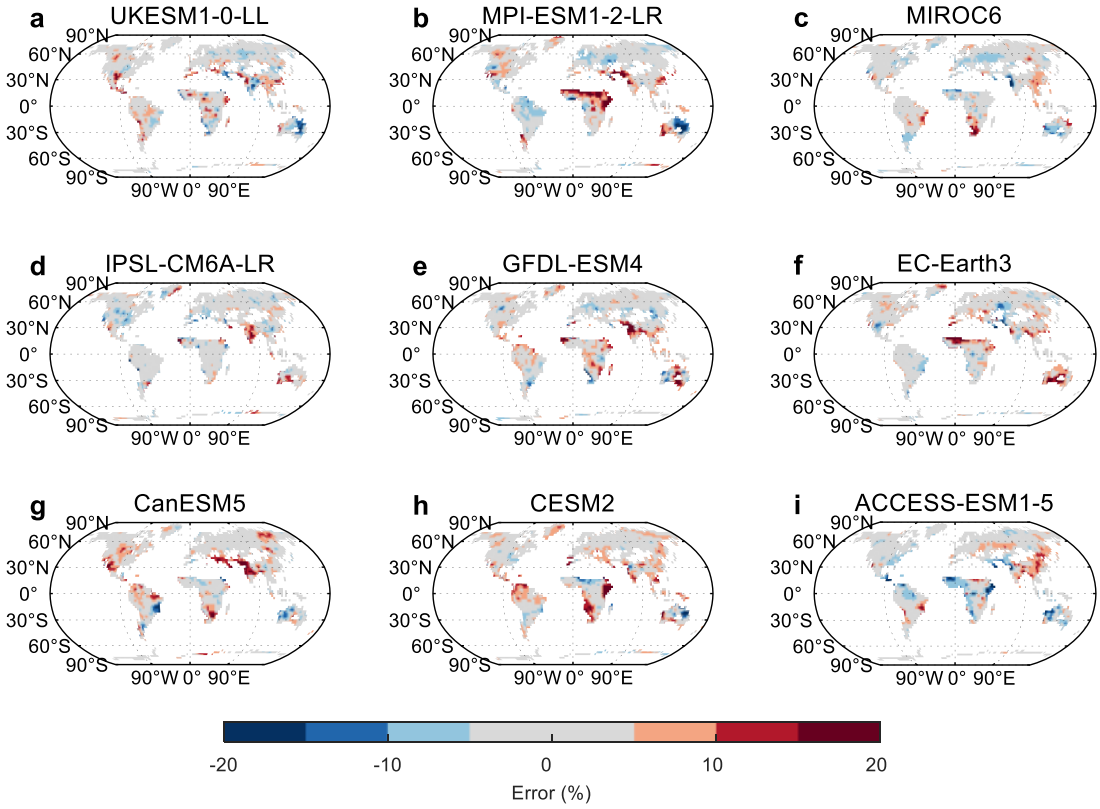

Figure S12. The spatial pattern of the MAP in 2071-2100 between each ESM and our emulation under the SSP5-8.5 scenario: **a**) UKESM1-0-LL; **b**) MPI-ESM1-2-LR; **c**) MIROC6; **d**) IPSL-CM6A-LR; **e**) GFDL-ESM4; **f**) EC-Earth3; **g**) CanESM5; **h**) CESM2; **i**) ACCESS-ESM1-5.

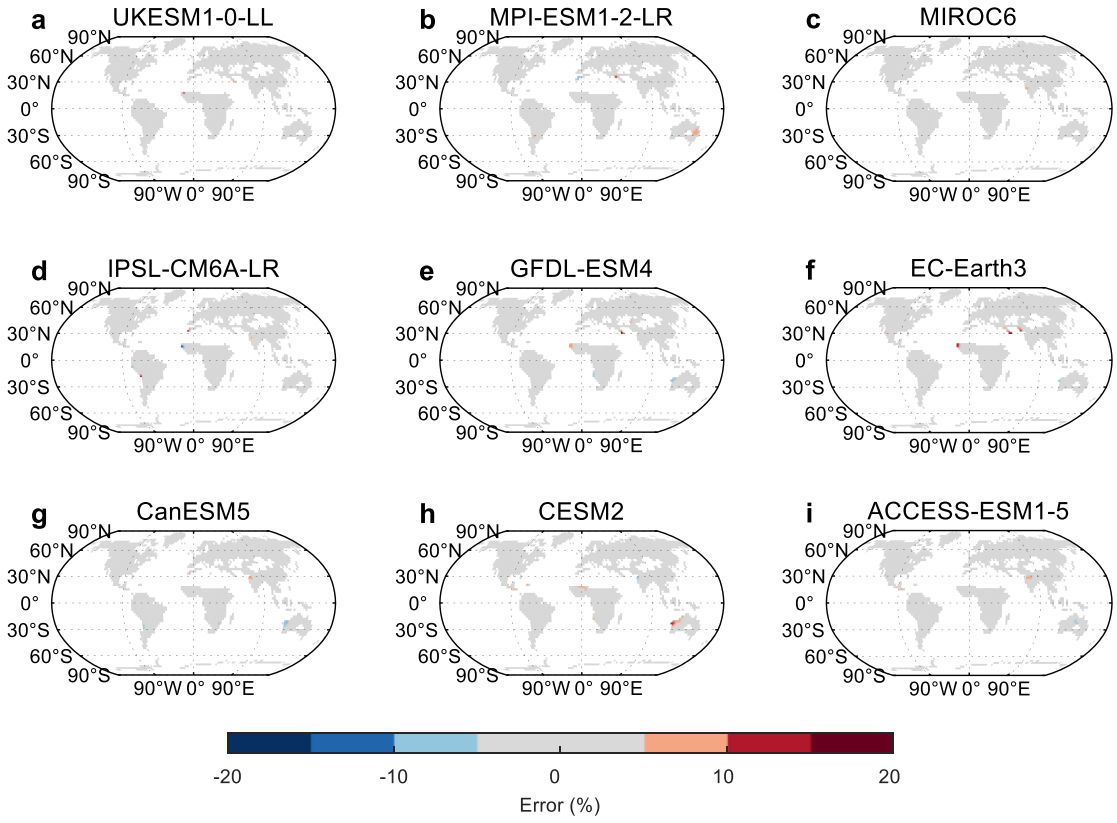

Figure S13. The spatial pattern of change in MAP between the period of 2015-2044 and 2071-2100 from **a**) UKESM1-0-LL and **b**) our emulation under SSP1-2.6 scenario. **c-d**) MPI-ESM1-2-LR; **e-f**) MIROC6; **g-h**) IPSL-CM6A-LR; **i-j)** GFDL-ESM4; **k-l**) EC-Earth3; **m-n**) CanESM5; **o-p**) CESM2; **q-r**) ACCESS-ESM1-5.

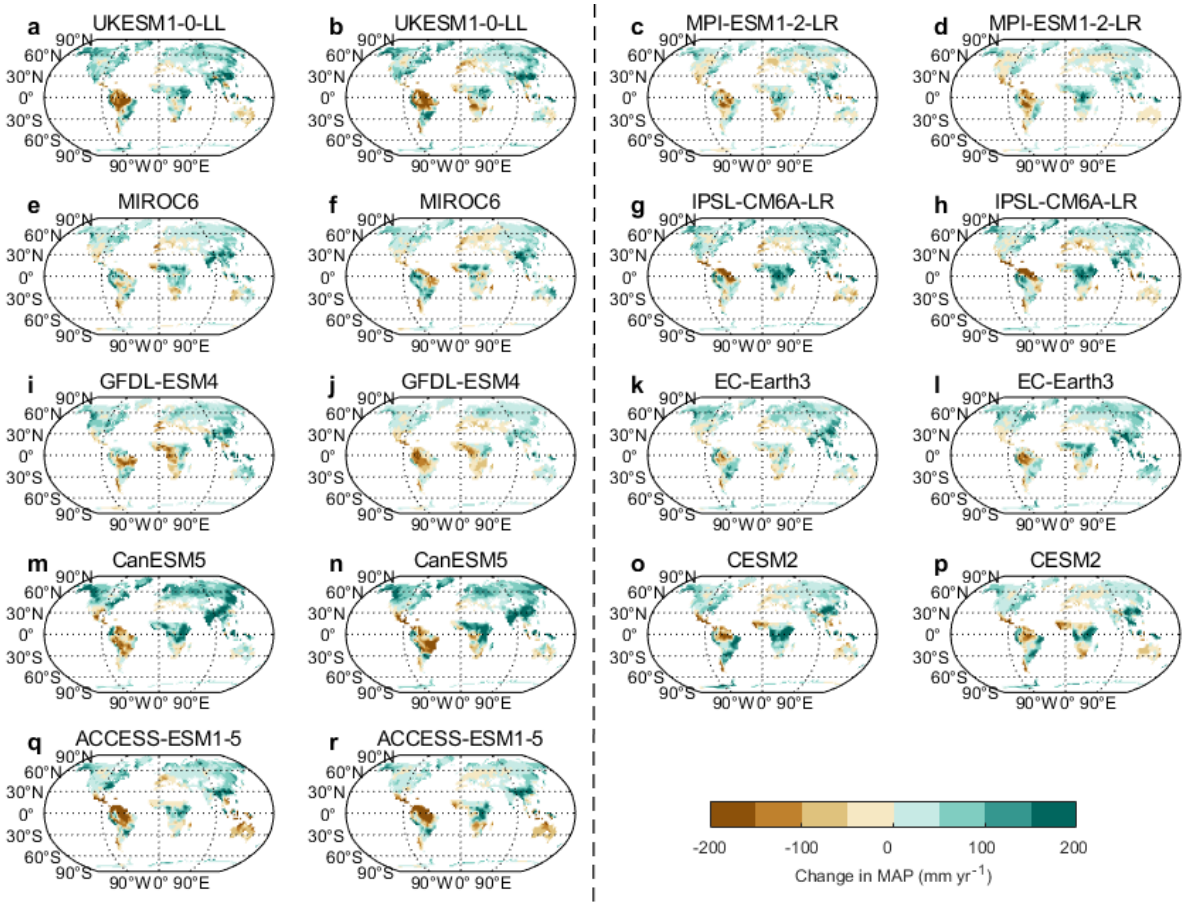

Figure S14. The spatial pattern of change in MAP between the period of 2015-2044 and 2071-2100 from **a**) UKESM1-0-LL and **b**) our emulation under SSP1-2.6 scenario. **c-d**) MPI-ESM1-2-LR; **e-f**) MIROC6; **g-h**) IPSL-CM6A-LR; **i-j)** GFDL-ESM4; **k-l**) EC-Earth3; **m-n**) CanESM5; **o-p**) CESM2; **q-r**) ACCESS-ESM1-5.

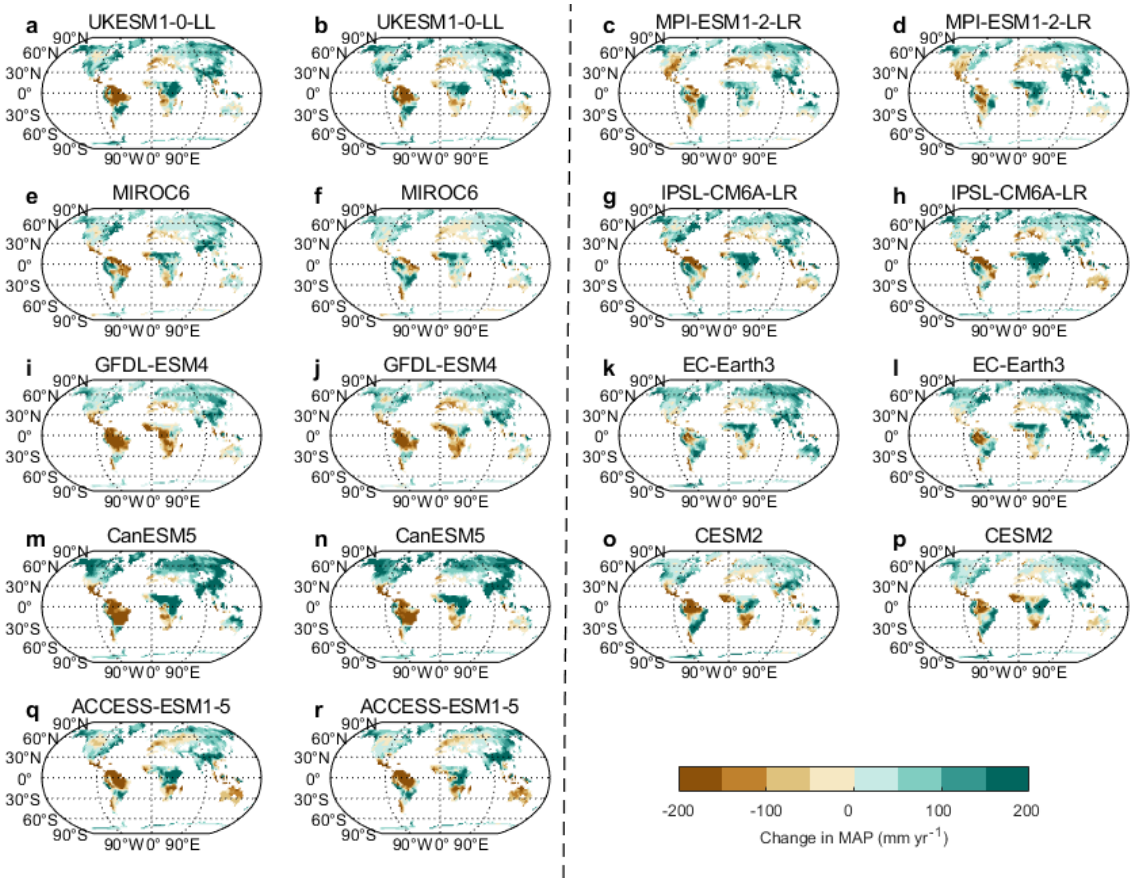

Figure S15. The spatial pattern of change in MAP between the period of 2015-2044 and 2071-2100 from **a**) UKESM1-0-LL and **b**) our emulation under SSP1-2.6 scenario. **c-d**) MPI-ESM1-2-LR; **e-f**) MIROC6; **g-h**) IPSL-CM6A-LR; **i-j)** GFDL-ESM4; **k-l**) EC-Earth3; **m-n**) CanESM5; **o-p**) CESM2; **q-r**) ACCESS-ESM1-5.

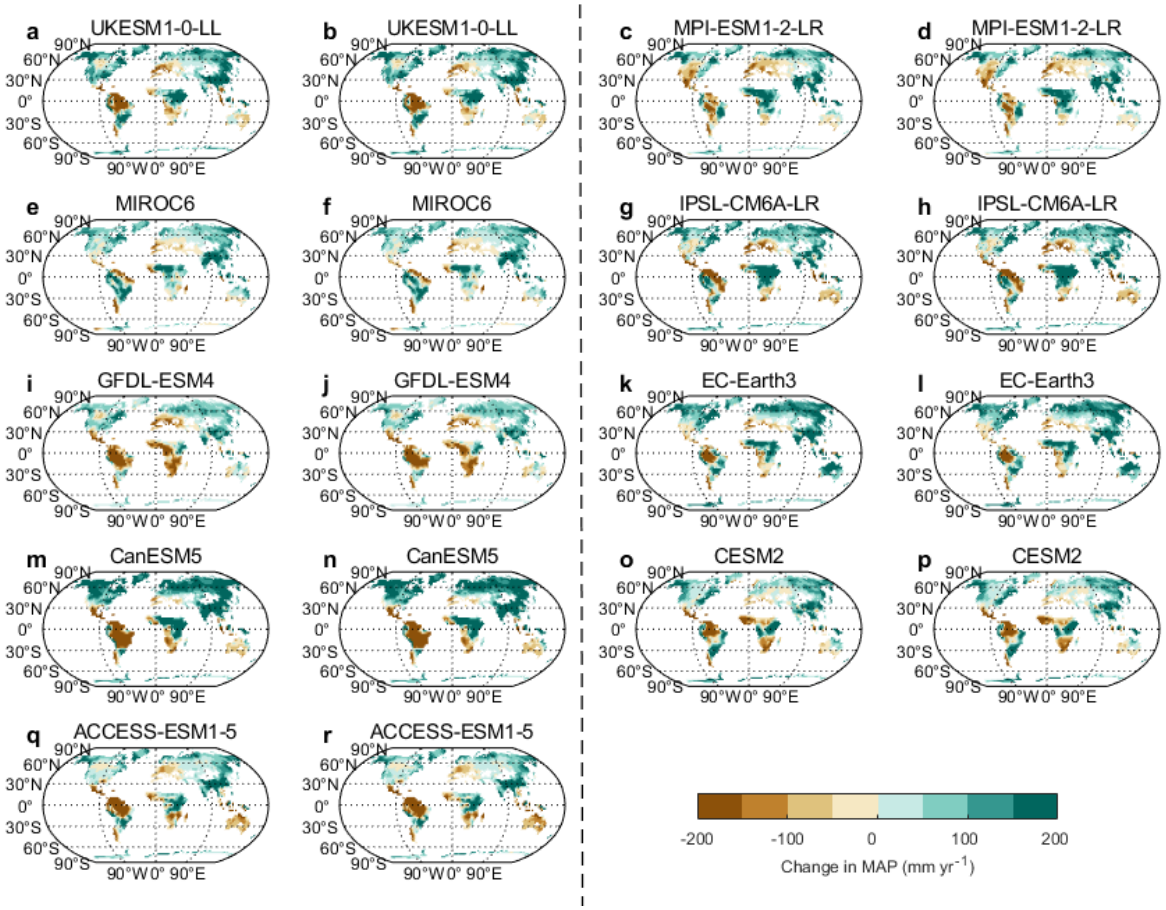

Figure S16. a) The spatial pattern of error of the three months average (March, April and May) in 1987-2016 between simple linear method and GSWP3; **b)** The spatial pattern of error of the spring average precipitation in 1987-2016 between PREMU and GSWP3; **c-d)** JJA (June, July, August); **e-f)** SON (September, October, November) ; **g-h)** DJF (December, January, February).

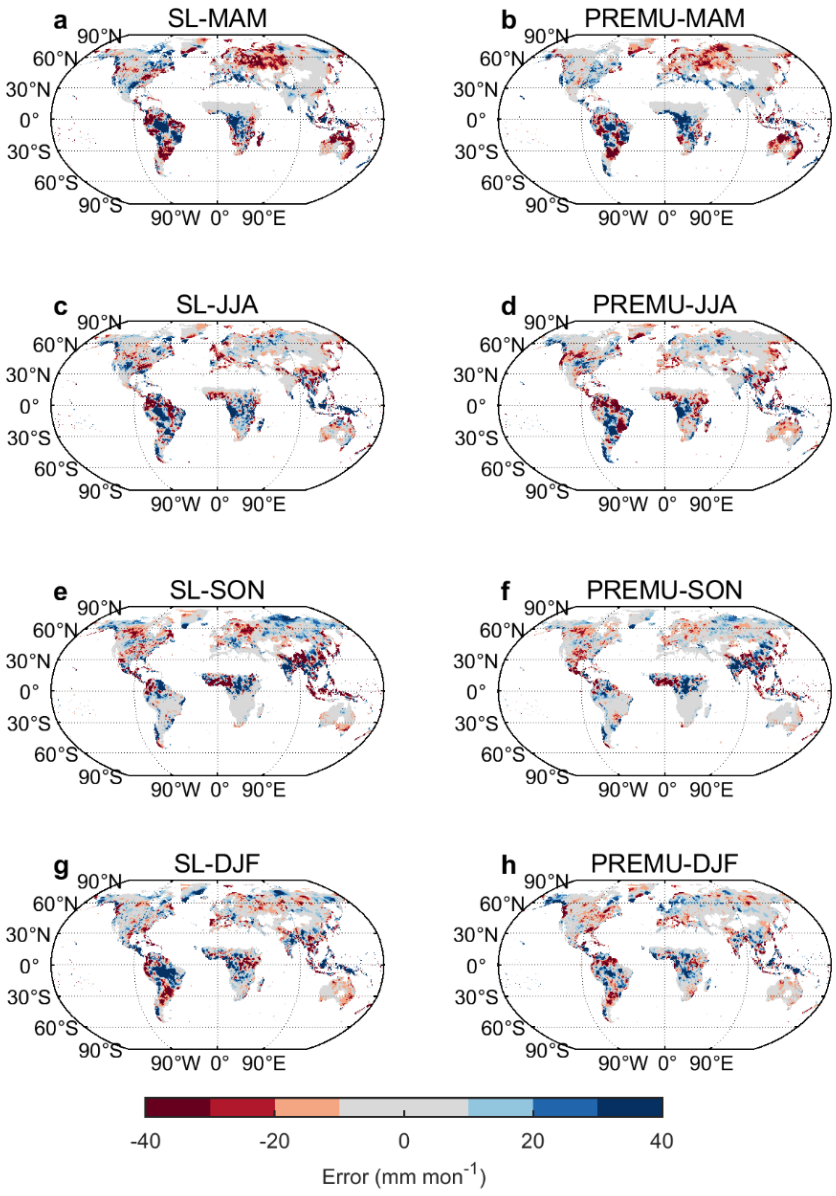

Figure S17. a) The seasonal cycle of multi-model mean 30° N-90° N latitude land average precipitation in 9 ESMs from CMIP6, and emulation from PREMU in 2071-2100 under SSP5-8.5; **b)** Eq.-30° N, **c)** 30° S-Eq., **d)** 90° S-30° S; **e-f)** SSP1-2.6; **i-l)** SSP2-4.5; **m-p)** SSP3-7.0.

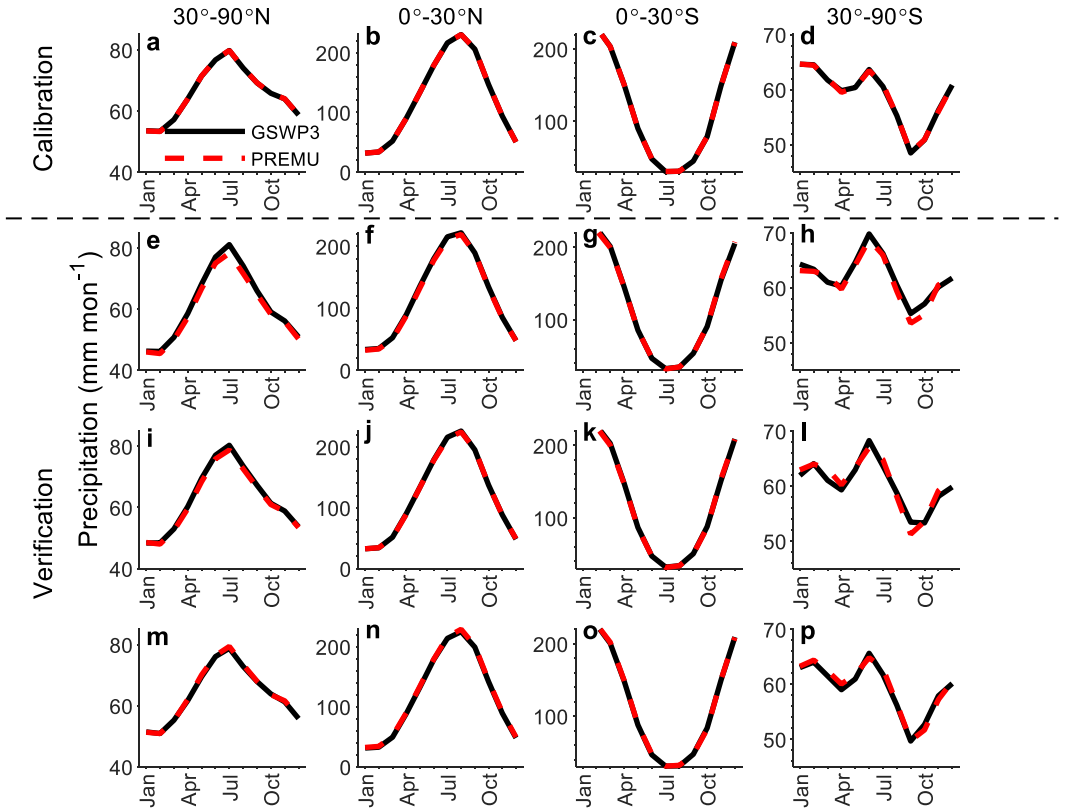

Figure S18. a) The spatial pattern of error of the three months average (March, April and July) precipitation in 2071-2100 between PREMU and ESMs under SSP5-8.5; **b)** JJA (June, July, August); **c)** SON (September, October, November) ; **d)** DJF (December, January, February); **e-f)** SSP1-2.6; **i-l)** SSP2-4.5; **m-p)** SSP3-7.0.

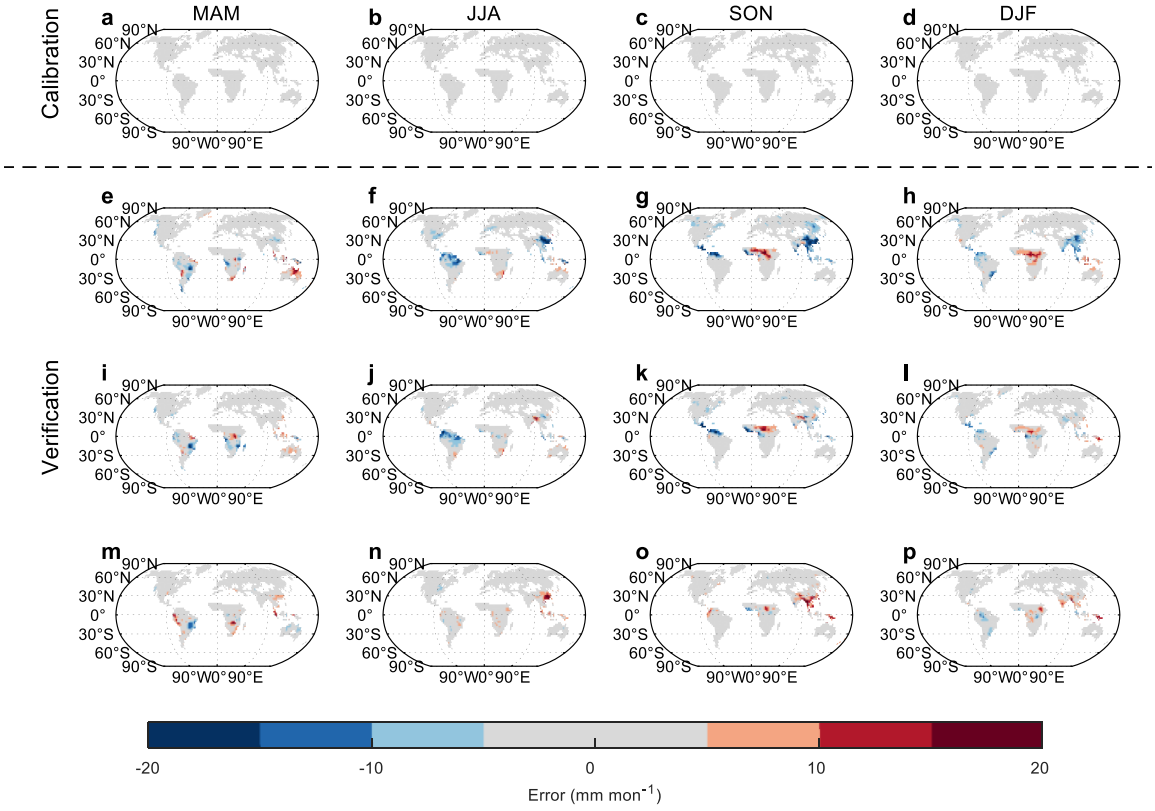

Figure S19. The comparison of average coefficients of the top 10 PCs in January under SSP5-8.5 (left column) and SSP1-2.6 (right column) after adjusting the order. The order of each column represents the PCs from top one to ten.

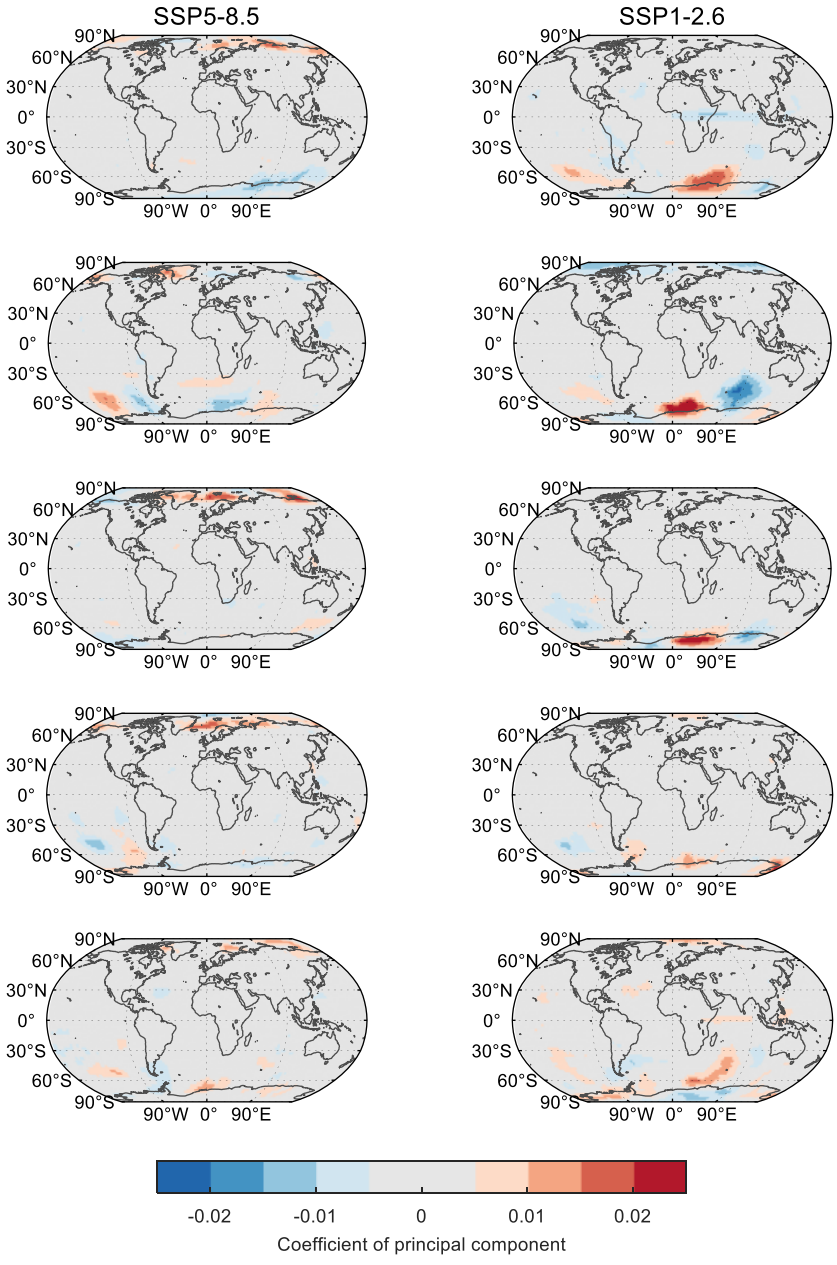

Figure S19. Continued.

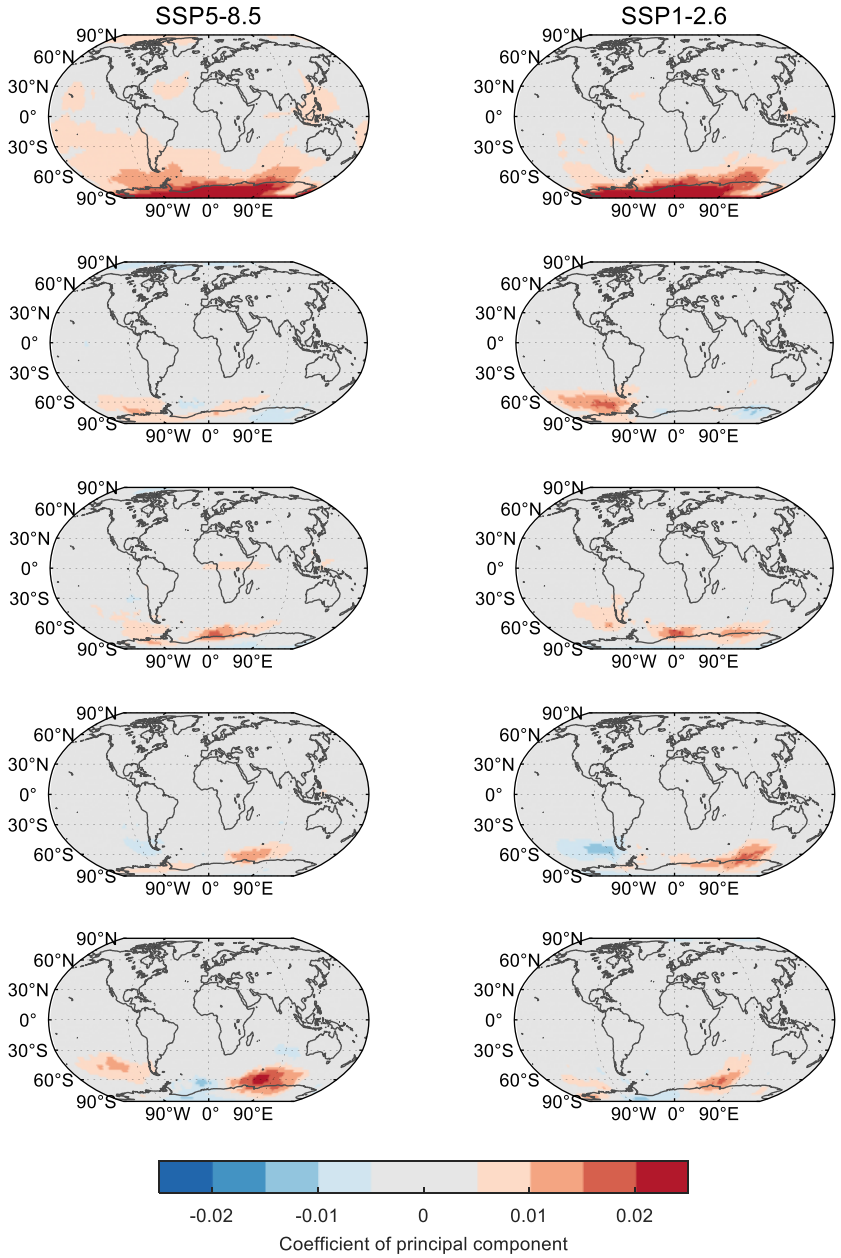

Figure S20. The comparison of average coefficients of the top 10 PCs in July under SSP5-8.5 and SSP1-2.6 after adjusting the order. The order of each column represents the PCs from top one to ten.

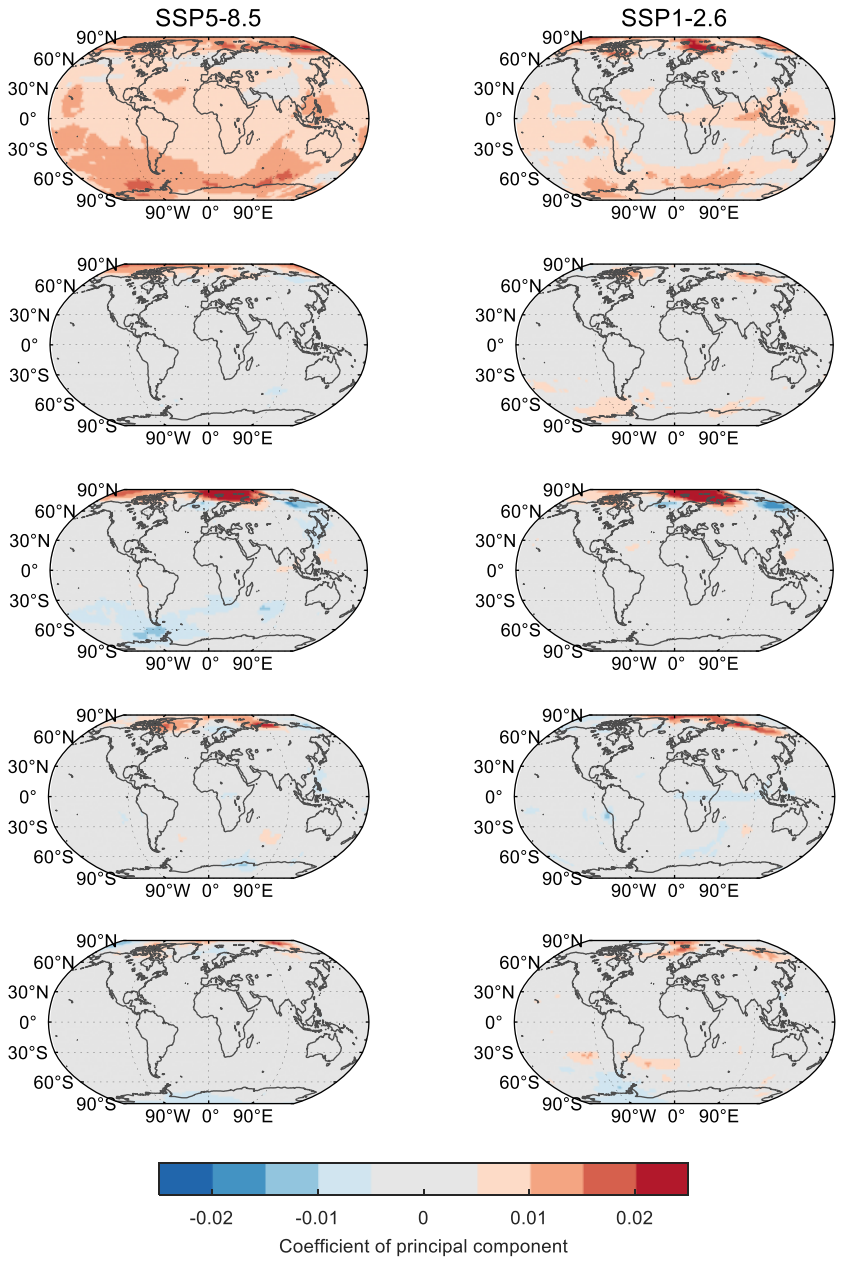

Figure S20. Continued.

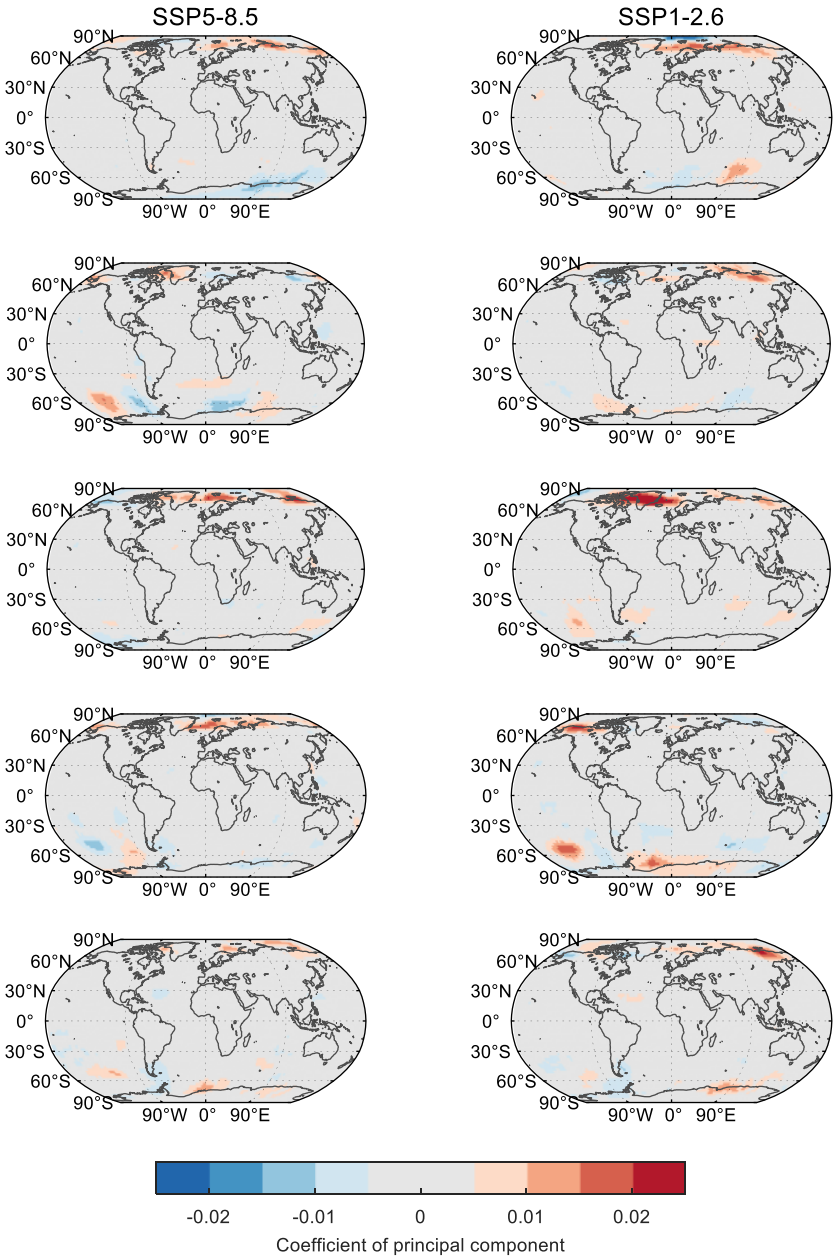

Figure S21. The emulation of PREMU based on only the top single PC of future precipitation: **a**) multi-model mean GLAP in 9 ESMs from CMIP6 (CMIP (9)), and the precipitation prediction by our emulator (PREMU- one PC) in 2015-2100 under the SSP5-8.5 scenario. The shaded area represents the mean±std. **b**) The spatial pattern of error in MAP during 2071-2100 between multi-model mean and our emulator. The emulation of precipitation under **c-d**) SSP1-2.6; **e-f**) SSP2-4.5; **g-h**) SSP3-7.0 by the PREMU- one PC calibrated under SSP5-8.5..

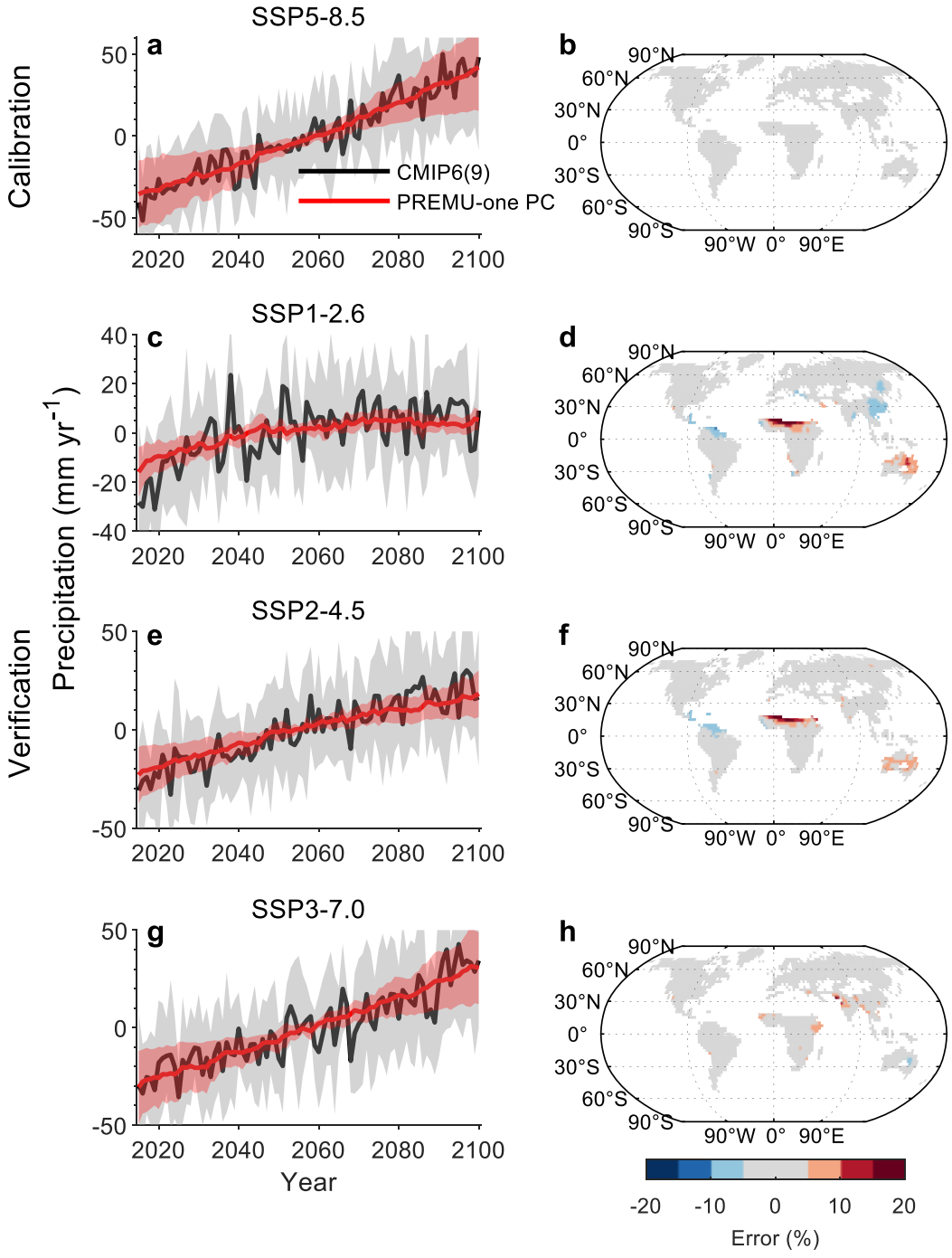

Figure S22. The GLAP in GSWP3 and the estimations from emulators based on monthly temperature (emulator-mon), 3-month average temperature (This study) and 6-month average temperature (emulator-6mon) in 1901-2016.

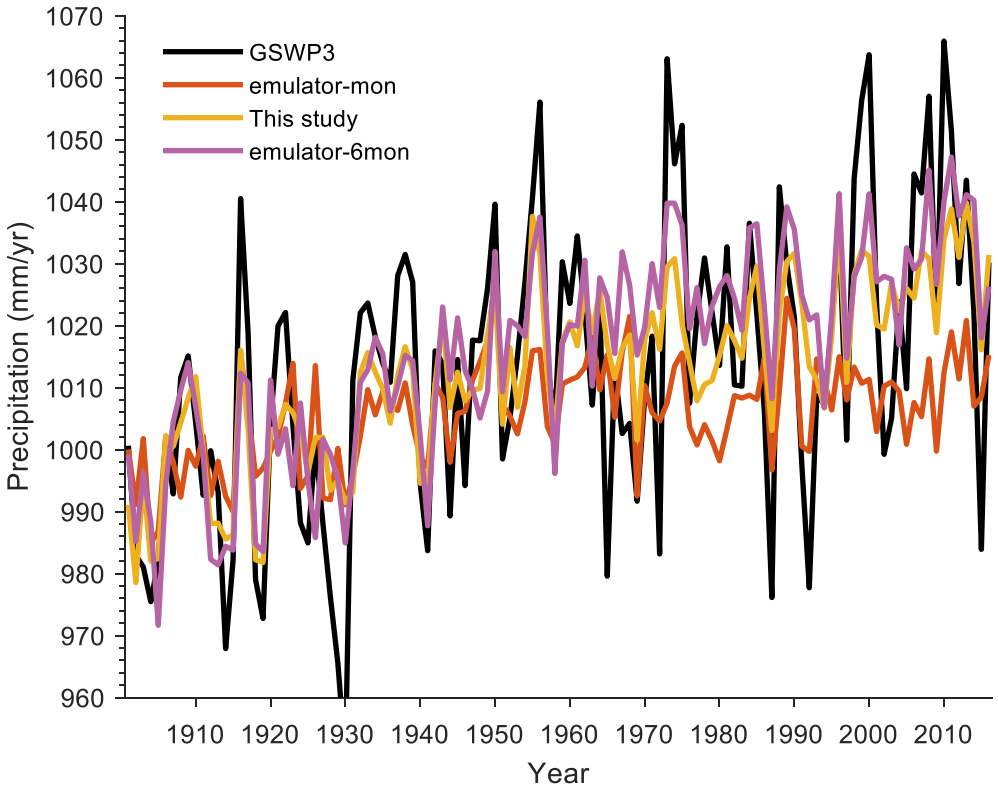

Figure S23. The emulation on future precipitation: **a**) multi-model mean GLAP in 9 ESMs from CMIP6 (CMIP (9)), and the precipitation prediction by the emulator-1mon (PREMU-mon) in 2015-2100 under the SSP5-8.5 scenario. The shaded area represents the mean±std. **b**) The spatial pattern of error in MAP during 2071-2100 between multi-model mean and our emulator. **c-d**) SSP1-2.6; **e-f**) SSP2-4.5; **g-h**) SSP3-7.0.

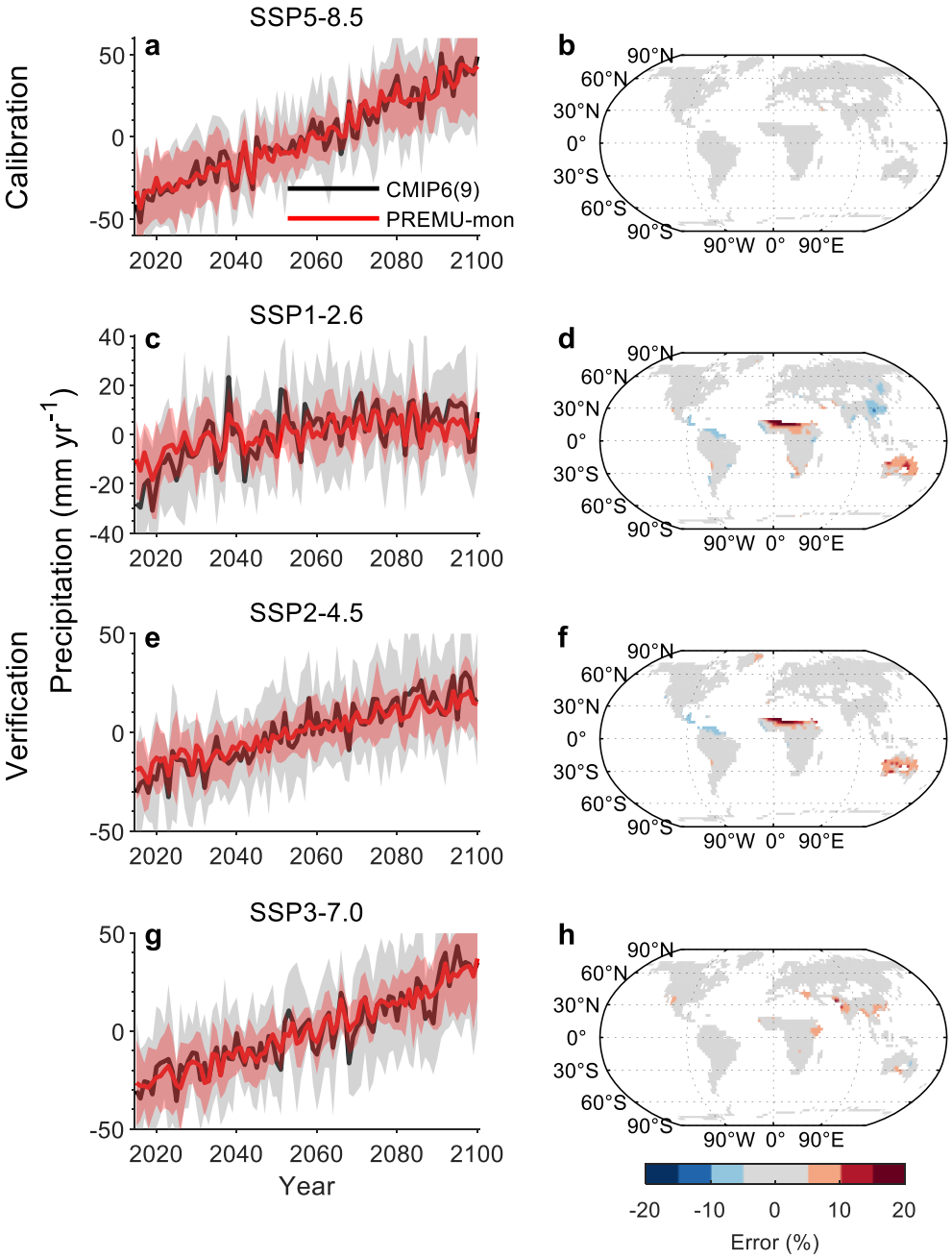

Figure S24. The emulation on future precipitation: **a**) multi-model mean GLAP in 9 ESMs from CMIP6 (CMIP (9)), and the precipitation prediction by the emulator-6mon (Emulator-6mon) in 2015-2100 under the SSP5-8.5 scenario. The shaded area represents the mean±std. **b**) The spatial pattern of error in MAP during 2071-2100 between multi-model mean and our emulator. **c-d**) SSP1-2.6; **e-f**) SSP2-4.5; **g-h**) SSP3-7.0.

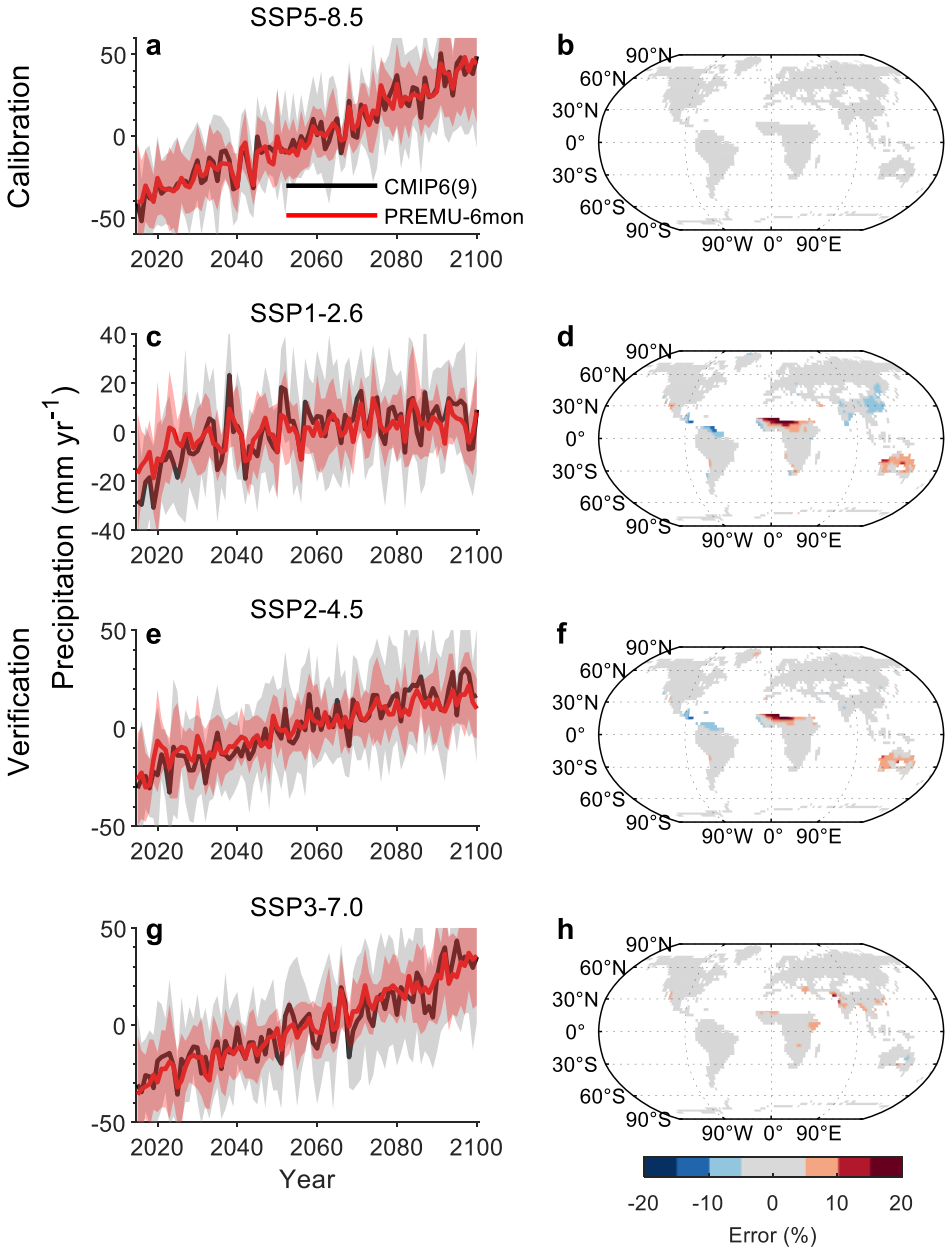

Figure S25. The emulation on future precipitation by emulator-land: **a**) multi-model mean GLAP in 9 ESMs from CMIP6 (CMIP (9)), and the precipitation prediction by emulator-land (PREMU-land) in 2015-2100 under the SSP5-8.5 scenario. The shaded area represents the mean±std. **b**) The spatial pattern of error in MAP during 2071-2100 between multi-model mean and our emulator. **c-d**) SSP1-2.6; **e-f**) SSP2-4.5; **g-h**) SSP3-7.0.

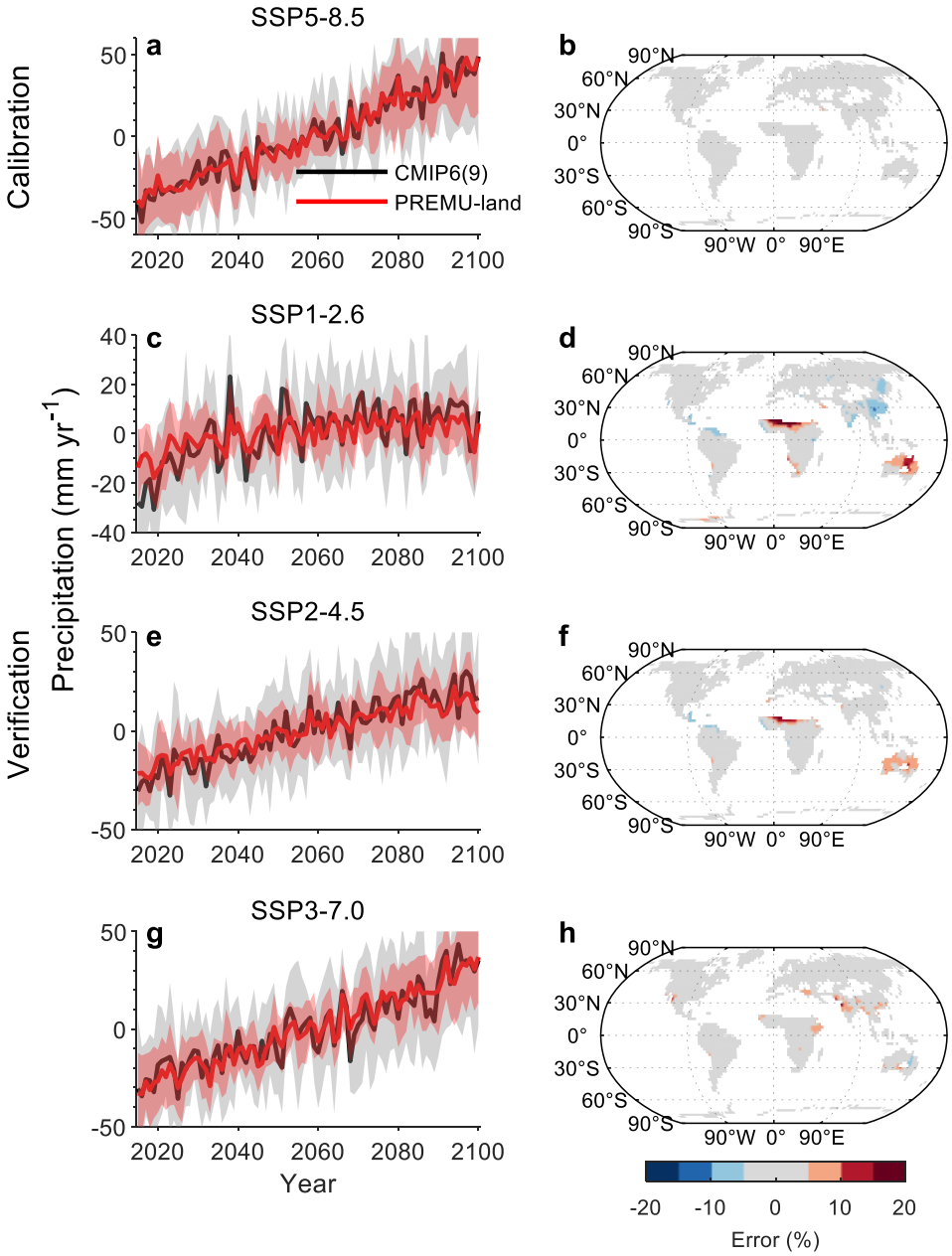

Figure S26. The spatial pattern of change in MAP in 2071-2100 from **a**) ESMs and **b**) emulation from emulator-land under SSP5-8.5 scenario. **c-d**) SSP1-2.6; **e-f**) SSP2-4.5; **g-h**) SSP3-7.0.